THE JOURNAL OF PHYSICAL CHEMISTRY Letters

pubs.acs.org/JPCL

Bistability and Hysteresis During Aggregation of Charged Nanoparticles

Dawei Wang,[†,‡,§] Bartlomiej Kowalczyk,[†,‡] István Lagzi,[†,‡] and Bartosz A. Grzybowski*[,†,‡]

[†]Department of Chemistry, and [‡]Department of Chemical and Biological Engineering, Northwestern University, 2145 Sheridan Road, Evanston, Illinois 60208 , and [§]School of Materials Science and Engineering, Northwestern Polytechnical University, Xi'an 710072, China

ABSTRACT Nanoparticles functionalized with ionizable ligands can exist in either dispersed or aggregated states at the same value of pH. This bistability and the related hystreresis accompanying pH changes derive from a subtle interplay between electrostatic and van der Waals forces. A theoretical model allows one to control the range of pH over which bistability is observed.

SECTION Nanoparticles and Nanostructures

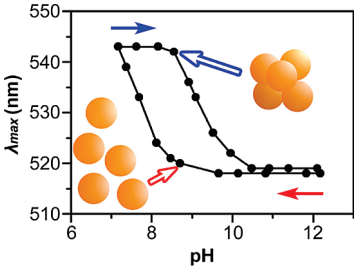

Aggregation phenomena in collections of nanoscopic particles are relevant to the synthesis of nanostructured materials,[1,2] and are important for the development of plasmonic nanosensors,[3−5] or nanoparticle (NP)-based drug delivery methods,[6,7] to name just a few. In most of the reported systems based on noncovalent interactions, only one state/form of aggregated NPs exists at the given values of system/thermodynamic parameters. This type of behavior is seen in ensembles of NPs interacting by van der Waals (vdW) forces,[8−10] and in most systems where aggregation is a function of temperature[11] or pH.[12,13] In few studies,[14−16] bistability deriving from the conformational changes of the NP ligands has been observed, but these effects have either been overlooked in the interpretation of results, or treated as experimentally undesirable artifacts. Nevertheless, bistability and the related phenomenon of hysteresis remain important for the development of, for instance, magnetic[17] and elastic[18] materials, and there has been recent interest in such systems at the nanoscale, mainly in conjunction with nanoelectronic[19,20] and delivery systems.[6,7] Here, we show that bistability and hysteresis can be "engineered" rationally into collections of charged NPs aggregating and dispersing in response to pH changes. These phenomena derive from a delicate balance between vdW and electrostatic interparticle interactions accounting for charge regulation on NP surfaces. The sum of these "component" potentials gives rise to an overall interaction potential that features an energy barrier at finite separations. Hysteresis comes about because overcoming the barrier from the aggregated into the dispersed and from the dispersed into the aggregated states requires different magnitudes of electrostatic interactions. These effects and the pH range over which hysteresis is observed can be controlled by varying the properties of the charged/ionizable ligands stabilizing the NPs and/or by changing particle sizes. NPs having two stable aggregation states at the same value of pH could be of interest in the context of NP-based memory devices and in delivery applications, where the particles (or their assemblies) migrate through nonuniform pH landscapes.

In a typical experiment, we used gold nanoparticles (AuNPs) with diameters of the metal cores of 10.0 ± 1.2 nm. These NPs were functionalized (Figure 1a) with a self-assembled monolayer (SAM)[21,22] of 2-fluoro-4-mercaptophenol (FMP, pK_a ∼ 8.3, ref 23) synthesized as described in the Supporting Information. The functionalized NPs were suspended in water at pH = 12.5 adjusted by the addition of tetramethylammonium hydroxide (TMAOH). Under these conditions, the NPs were fully charged (surface potential $\zeta \sim -61.2$ mV) and unaggregated as evidenced by the dynamic light scattering (DLS) measurements illustrated in Figure 1b and also by the surface plasmon resonance (SPR) maxima at $\lambda_{max} \sim 524$ nm, characteristic of free AuNPs (Figure 1c). When the pH was lowered and the phenol groups became protonated, the NPs gradually aggregated, with the most prominent red shift of λ_{max} occurring below pH ∼ 8 (Figure 1d). At pH ∼ 7.0, the particles formed aggregates ∼100 nm in diameter (by DLS), with $\lambda_{max} \sim 539$ nm, and surface potential ∼ − 46.9 mV (note: below pH ∼ 7, particles precipitated). Remarkably, when the pH was subsequently increased, the NPs initially remained aggregated and became fully dispersed only at pH's higher than ∼11. The same trends were observed on subsequent pH cycles (Figure 1d). Overall, the NPs exhibited pronounced hysteresis and in the range of pH between ∼7.5 and ∼9.5 showed distinct bistability; that is, either aggregated or unaggregated NP "states" could exist at a given value of pH depending on how this value was reached. The two states were stable for at least 6 months during which the solutions showed no spectral changes.

The observed phenomena are due to a subtle interplay between electrostatic repulsions and vdW attractions between the NPs. Qualitatively, if these interactions are of

Received Date: March 28, 2010
Accepted Date: April 12, 2010
Published on Web Date: April 19, 2010

DOI: 10.1021/jz100406w | *J. Phys. Chem. Lett.* **2010**, *1*, 1459–1462

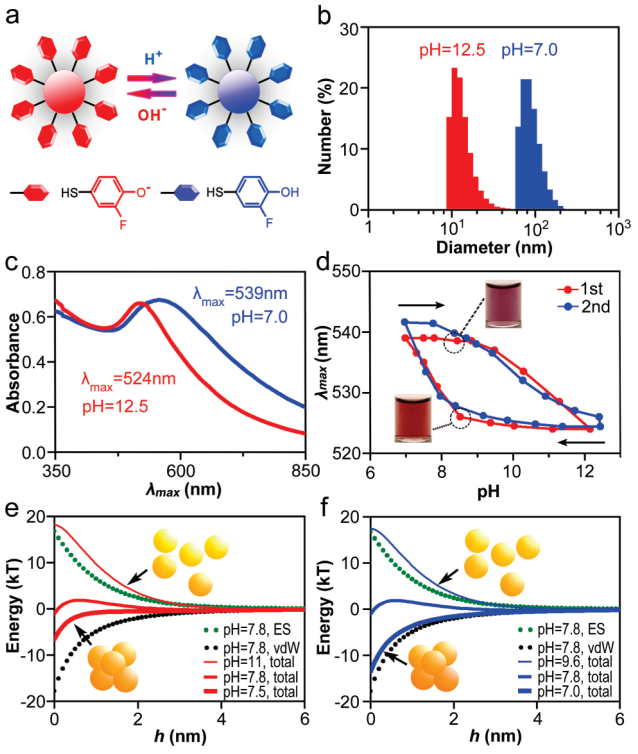

Figure 1. (a) Schematic representation of the FMP-coated AuNPs used in the experiments. The NPs are unaggregated at high pH due to electrostatic repulsions between deprotonated FMP SAMs. At low pH, strong vdW forces dominate and the NPs aggregate. This behavior is visualized by the color change of the NP solution from red (free NPs) to blue-violet (aggregated NPs). (b) Hydrodynamic radii measured by DLS and (c) UV−vis spectra of 10 nm NPs at high and low pH's. (d) Experimental data showing two consecutive hysteresis loops for 10 nm AuFMP NPs. Similar loops are observed on consecutive cycles (up to seven were tested). The insert images show NP solutions that, depending on how the sample was prepared, can exist at the same pH (here, 8.3). Calculated interaction potentials between (e) aggregating and (f) dispersed NPs as a function of distance, h, between particle surfaces. The legends specify the pH and type of interaction (ES = electrostatic, vdW = van der Waals; total = ES + vdW).

similar magnitudes, the net potential exhibits a maximum/barrier at some finite separation (Figure 1e). As long as this maximum is present, it prevents the NPs from aggregating. When, however, the pH is lowered and the electrostatic repulsions weaken, the barrier becomes smaller and, at some critical value, pH_{agg}, is no longer present, making the potential monotonically decrease with decreasing interparticle separation and allowing the NPs to aggregate (Figure 1e, thick red curve for pH = 7.5). Once the NPs are in the aggregated state, their disassembly requires that they "get out" of a deep potential well. In order to do so, however, the pH and the electrostatic repulsions have to increase to the point where the net potential becomes monotonically decreasing with particle separation; importantly, this condition requires pH_{dis} higher than pH_{agg} (e.g., Figure 1f, thin blue curve for pH = 9.6), and the system exhibits hysteresis.

These arguments can be quantified by a model assuming pairwise interactions between the NPs (for justification of this assumption, see ref 8). The vdW energy is primarily due to the interactions between NPs' metal cores,[24] and is given by

$$u_{vdW}(h) = -\frac{A}{3}\left[\frac{R_c^2}{(2R+h)^2-4R_c^2}+\frac{R_c^2}{(2R+h)^2}+\frac{1}{2}\ln\left(1-\frac{4R_c^2}{(2R+h)^2}\right)\right] \quad (1)$$

where $A = 4 \times 10^{-19}$ J is the Hamaker constant for gold across water,[25] R_c is the radius of the metal core, R is the NP radius (core plus SAM thickness, ~ 0.5 nm), and h is the separation between NP surfaces. Electrostatic interactions between charged NPs in ionic solution are derived from the appropriate electrostatic potentials, φ, via thermodynamic integration[26,27] and account for "charge regulation" at the NPs' surfaces.[24,28] Briefly, the electrostatic potential around an NP, φ, is well approximated by the linearized Poisson−Boltzmann (PB) equation, $\nabla^2\varphi = \kappa^2\varphi$, where $\kappa^{-1} = (\varepsilon\varepsilon_0 k_B T/2N_A c_s e^2)^{1/2}$ is the Debye screening length, ε is the relative permittivity of the solvent ($\varepsilon \approx 80$ for water), ε_0 is the vacuum permittivity, k_B is the Boltzmann constant, T is the temperature ($T \approx 298$ K in our experiments), N_A is the Avogadro constant, c_s is the monovalent salt concentration (here, $c_s \approx 0.1$ mol/L), and e is the elementary charge. The density of deprotonated FMPs on NP surface, Γ, is given by $\Gamma = \Gamma_0/(1 + 10^{pK_a - pH})$, where Γ_0 is the surface density of all ligands (both protonated and deprotonated; $\Gamma_0 \approx 4.7$ nm^{-2} for SAM on AuNPs[29]). The equilibrium between counterions (here, tetramethylammonium cations, TMA^+) adsorbed onto the charged NP surface and those free in solution is determined by $N_{A^-}x_{B^+}/N_{AB} = \exp[-(\Delta G_d - e\varphi_s)/k_B T]$, where N_{A^-} and N_{AB} are the numbers of counterion-free deprotonated FMP ligands and counterion-bound deprotonated FMP ligands, respectively, x_{B^+} is the mole fraction of counterions (note: the concentration of H^+ at pH ≈ 6−13 is ~10^{-6} to 10^{-13} mol/L, which is negligible compared to the concentration of TMA^+, ~ 0.1 mol/L), ΔG_d is the free energy of ion dissociation in the absence of any external fields ($\Delta G_d \approx 2.1 \times 10^{-20}$ J),[8] and φ_s is the electrostatic potential at the NP surface. Thus, the surface charge density, σ, may be expressed as $\sigma = -e\Gamma/\{1 + x_{B^+}\exp[(\Delta G_d - e\varphi_s)/k_B T]\}$. Since the relative permittivity of a SAM ($\varepsilon_{SAM} \approx 2$, ref 29) is small compared to that of water (the solvent in our experiments), the surface charge density may also be written as $\sigma = -\varepsilon\varepsilon_0 \nabla\varphi_s \cdot \vec{n}$, where $\vec{n}$ is the outward surface normal. The boundary conditions at NPs' surfaces are linearized about the potential of an isolated NP, φ_∞, such that $-\varepsilon\varepsilon_0 \nabla\varphi_s \cdot \vec{n} = S - C\varphi_\infty$, where $S = \sigma(\varphi_\infty) - (\partial\sigma/\partial\varphi)_\infty\varphi_\infty$ and $C = -(\partial\sigma/\partial\varphi)_\infty$. After some algebra, the electrostatic interaction energy between two like-charged NPs can be derived as

$$u_{ES}(h) = \pi\varepsilon\varepsilon_0 R\left[\frac{\phi_s^2}{\Delta}\times\ln(1-\Delta^2 e^{-2\kappa h})+\frac{2\phi_s^2}{|\Delta|}\times\arctan(|\Delta|e^{-\kappa h})\right] \quad (2)$$

where the coefficient $\Delta = (C - \varepsilon\varepsilon_0\kappa)/(C + \varepsilon\varepsilon_0\kappa)$ depends on $C = -\partial\sigma/\partial\varphi\,|_{\varphi=\varphi_\infty}$,[8] which is the derivative of the surface charge with respect to the potential of an isolated NP, φ_∞.

DOI: 10.1021/jz100406w | J. Phys. Chem. Lett. 2010, 1, 1459–1462

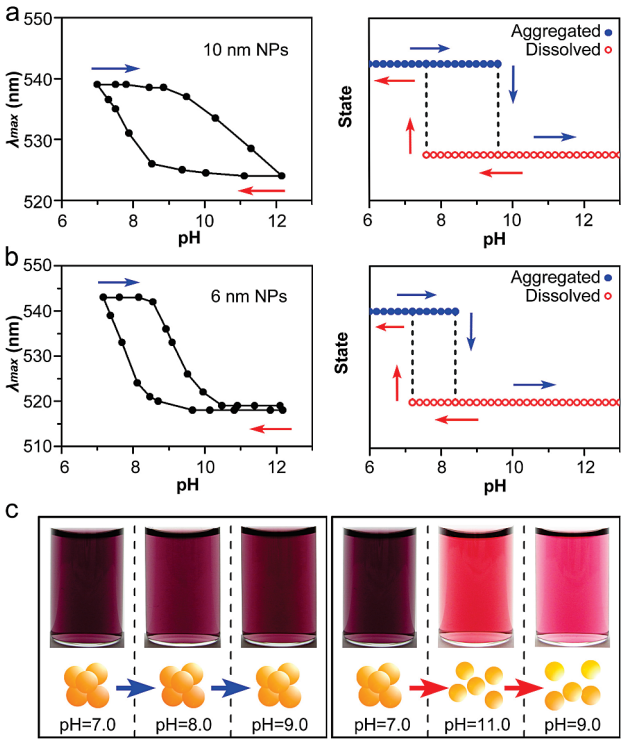

Figure 2. Experimental (left) and calculated (right) hysteresis loops for (a) 10 nm, and (b) 6 nm AuFMP NPs. (c) Illustration of an experiment in which the final state of AuFMPs depends on the pH "route" the NPs "travelled". Here, the NPs are initially prepared at pH = 7 (aggregated state, violet color) and are then transferred to solutions of different pH's. The final, pH = 9 state depends on whether the NPs "passed" through a high-pH region: if they did not (left panel), the final state is that of aggregated NPs; if they did (right panel), the final state comprises dispersed particles (red color).

The total interaction potential is then $u(h) = u_{vdW}(h) + u_{ES}(h)$. The aggregation condition upon lowering pH is therefore $du(h)/dh > 0$ for all values of h (i.e., no potential maximum/barrier). Similarly, the condition for the disassembly of aggregated NPs is $du(h)/dh|_{h=0} < 0$ (i.e., potential monotonically decreasing/purely repulsive). Figure 2a illustrates that, upon substitution of pertinent experimental parameters ($R_c \approx 5.0$ nm, $R \approx 5.5$ nm, $\varepsilon \approx 80$, $pK_a \approx 8.3$), this model predicts hysteretic behavior of the system with the threshold pH's for aggregation and disassembly close to those observed in experiments.

One of the major virtues of this simple theoretical model is that it can guide the design of NP systems exhibiting bistability over different ranges of pH. For example, upon decreasing particle diameter (other parameters kept constant), bistability is expected to occur over a narrower pH range. This is corroborated by the experiments illustrated in Figure 2b where 6.0 nm AuFMP NPs show hysteretic behavior between pH ~ 7.3 and 8.8, which agrees with the theoretically predicted range of pH ~ 7.2−8.5.

Our last comment concerns the influence on the SAM molecules on the system's behavior. Because, as argued above, bistability derives from an interplay between vdW and electrostatic forces, the magnitudes of these interactions need to be commensurate. The short ligands used here allow for close approach of the metal cores and relatively large vdW interactions. With the same NPs but longer ligands in which FMP moieties are spaced from the Au surface by alkane chains, the vdW forces are weaker, and hysteresis effect is either very weak or absent (e.g., no hystreresis observed in experiments with C_{11} FMP thiols). Also, the presence of other types of interactions is important, as evidenced by experiments with NPs covered with benzoate (4-mercaptobenzoic acid) rather than phenolate (FMP) ligands; for the former, NP aggregation is irreversible, likely due to strong hydrogen bonding between the carboxylic acids and/or bridging[30] of these groups by ions present in solution.

In summary, implementation of bistable NP systems requires careful optimization of interparticle interactions. We suggest that such systems might prove useful is NP-based delivery, where NP aggregates prepared at appropriate pH disperse only if moving along desired pH "landscapes". One example of such a situation is illustrated in Figure 2c, where the final state of NPs at pH = 9 depends on whether or not they passed through an intermediate, high-pH region.

SUPPORTING INFORMATION AVAILABLE Synthesis of AuNPs and their functionalization with FMP thiols. This material is available free of charge via the Internet at http://pubs.acs.org.

AUTHOR INFORMATION

Corresponding Author:

*To whom correspondence should be addressed. E-mail: grzybor@northwestern.edu.

ACKNOWLEDGMENT This work was supported by the Non-equilibrium Energy Research Center, which is an Energy Frontier Research Center funded by the U.S. Department of Energy, Office of Science, Office of Basic Energy Sciences, under Award DESC0000989.

REFERENCES

(1) Shevchenko, E. V.; Talapin, D. V.; Kotov, N. A.; O'Brien, S.; Murray, C. B. Structural Diversity in Binary Nanoparticle Superlattices. *Nature* **2006,** *439*, 55–59.

(2) Klajn, R.; Bishop, K. J. M.; Fialkowski, M.; Paszewski, M.; Campbell, C. J.; Gray, T. P.; Grzybowski, B. A. Plastic and Moldable Metals by Self-Assembly of Sticky Nanoparticle Aggregates. *Science* **2007,** *316*, 261–264.

(3) Elghanian, R.; Storhoff, J. J.; Mucic, R. C.; Letsinger, R. L.; Mirkin, C. A. Selective Colorimetric Detection of Polynucleotides Based on the Distance-Dependent Optical Properties of Gold Nanoparticles. *Science* **1997,** *277*, 1078–1081.

(4) Lee, J. S.; Ulmann, P. A.; Han, M. S.; Mirkin, C. A. A DNA−Gold Nanoparticle-Based Colorimetric Competition Assay for the Detection of Cysteine. *Nano Lett.* **2008,** *8*, 529–533.

(5) Niemeyer, C. M. Nanoparticles, Proteins, and Nucleic Acids: Biotechnology Meets Materials Science. *Angew. Chem., Int. Ed.* **2001,** *40*, 4128–4158.

(6) Nam, J.; Won, N.; Jin, H.; Chung, H.; Kim, S. pH-Induced Aggregation of Gold Nanoparticles for Photothermal Cancer Therapy. *J. Am. Chem. Soc.* **2009,** *131*, 13639–13645.

DOI: 10.1021/jz100406w | *J. Phys. Chem. Lett.* **2010,** *1*, 1459–1462

(7) Tsapis, N.; Bennett, D.; Jackson, B.; Weitz, D. A.; Edwards, D. A. Trojan Particles: Large Porous Carriers of Nanoparticles for Drug Delivery. *Proc. Natl. Acad. Sci. U.S.A.* **2002,** *99*, 12001–12005.
(8) Bishop, K. J. M.; Kowalczyk, B.; Grzybowski, B. A. Precipitation of Oppositely Charged Nanoparticles by Dilution and/or Temperature Increase. *J. Phys. Chem. B* **2009,** *113*, 1413–1417.
(9) Zhou, J.; Beattie, D. A.; Ralston, J.; Sedev, R. Colloid Stability of Thymine-Functionalized Gold Nanoparticles. *Langmuir* **2007,** *23*, 12096–12103.
(10) Valignat, M. P.; Theodoly, O.; Crocker, J. C.; Russel, W. B.; Chaikin, P. M. Reversible Self-Assembly and Directed Assembly of DNA-Linked Micrometer-Sized Colloids. *Proc. Natl. Acad. Sci. U.S.A.* **2005,** *102*, 4225–4229.
(11) Nykypanchuk, D.; Maye, M. M.; van der Lelie, D.; Gang, O. DNA-Guided Crystallization of Colloidal Nanoparticles. *Nature* **2008,** *451*, 549–552.
(12) Si, S.; Mandal, T. K. pH-Controlled Reversible Assembly of Peptide-Functionalized Gold Nanoparticles. *Langmuir* **2007,** *23*, 190–195.
(13) Isojima, T.; Lattuada, M.; Vander Sande, J. B.; Hatton, T. A. Reversible Clustering of pH- and Temperature-Responsive Janus Magnetic Nanoparticles. *ACS Nano* **2008,** *2*, 1799–1806.
(14) Guo, Y.; Ma, Y. D.; Xu, L.; Li, J.; Yang, W. S. Conformational Change Induced Reversible Assembly/Disassembly of Poly-L-lysine-Functionalized Gold Nanoparticles. *J. Phys. Chem. C* **2007,** *111*, 9172–9176.
(15) Ye, J.; Hou, Y.; Zhang, G. Z.; Wu, C. Temperature-Induced Aggregation of Poly(*N*-isopropylacrylamide)-Stabilized CdS Quantum Dots in Water. *Langmuir* **2008,** *24*, 2727–2731.
(16) Viudez, A. J.; Madueno, R.; Pineda, T.; Blazquez, M. Stabilization of Gold Nanoparticles by 6-Mercaptopurine Monolayers: Effects of the Solvent Properties. *J. Phys. Chem. B* **2006,** *110*, 17840–17847.
(17) Mannini, M.; Pineider, F.; Sainctavit, P.; Danieli, C.; Otero, E.; Sciancalepore, C.; Talarico, A. M.; Arrio, M.-A.; Cornia, A.; Gatteschi, D.; Sessoli, R. Magnetic Memory of a Single-Molecule Quantum Magnet Wired to a Gold Surface. *Nat. Mater.* **2009,** *8*, 194–197.
(18) Ghatak, A.; Mahadevan, L. Solenoids and Plectonemes in Stretched and Twisted Elastomeric Filaments. *Phys. Rev. Lett.* **2005,** *95*, 057801.
(19) Kim, T. H.; Jang, E. Y.; Lee, N. J.; Choi, D. J.; Lee, K.-J.; Jang, J.-t.; Choi, J.-s.; Moon, S. H.; Cheon, J. Nanoparticle Assemblies as Memristors. *Nano Lett.* **2009,** *9*, 2229–2233.
(20) Leong, W. L.; Lee, P. S.; Lohani, A.; Lam, Y. M.; Chen, T.; Zhang, S.; Dodabalapur, A.; Mhaisalkar, S. G. Non-Volatile Organic Memory Applications Enabled by In Situ Synthesis of Gold Nanoparticles in a Self-Assembled Block Copolymer. *Adv. Mater.* **2008,** *20*, 2325–2331.
(21) Witt, D.; Klajn, R.; Barski, P.; Grzybowski, B. A. Applications, Properties and Synthesis of ω-Functionalized *n*-Alkanethiols and Disulfides — The Building Blocks of Self-Assembled Monolayers. *Curr. Org. Chem.* **2004,** *8*, 1763–1797.
(22) Love, J. C.; Estroff, L. A.; Kriebel, J. K.; Nuzzo, R. G.; Whitesides, G. M. Self-Assembled Monolayers of Thiolates on Metals as a Form of Nanotechnology. *Chem. Rev.* **2005,** *105*, 1103–1170.
(23) Han, J.; Tao, F.-M. Correlations and Predictions of pKa Values of Fluorophenols and Bromophenols Using Hydrogen-Bonded Complexes with Ammonia. *J. Phys. Chem. A* **2005,** *110*, 257–263.
(24) Bishop, K. J. M.; Grzybowski, B. A. "Nanoions": Fundamental Properties and Analytical Applications of Charged Nanoparticles. *ChemPhysChem* **2007,** *8*, 2171–2176.
(25) Israelachvili, J. N. *Intermolecular and Surface Forces*, 2nd ed.; Academic Press: New York, 1991.
(26) Carnie, S. L.; Chan, D. Y. C.; Gunning, J. S. Electrical Double Layer Interaction between Dissimilar Spherical Colloidal Particles and between a Sphere and a Plate: The Linearized Poisson—Boltzmann Theory. *Langmuir* **1994,** *10*, 2993–3009.
(27) Verwey, E. J. W.; Overbeek, J. T. G. *Theory of the Stability of Lyophobic Colloids*; Elsevier: New York, 1948.
(28) Bishop, K. J. M.; Wilmer, C. E.; Soh, S.; Grzybowski, B. A. Nanoscale Forces and Their Uses in Self-Assembly. *Small* **2009,** *5*, 1600–1630.
(29) Leff, D. V.; Ohara, P. C.; Heath, J. R.; Gelbart, W. M. Thermodynamic Control of Gold Nanocrystal Size: Experiment and Theory. *J. Phys. Chem.* **1995,** *99*, 7036–7041.
(30) Ojea-Jimenez, I.; Puntes, V. Instability of Cationic Gold Nanoparticle Bioconjugates: The Role of Citrate Ions. *J. Am. Chem. Soc.* **2009,** *131*, 13320–13327.

DOI: 10.1021/jz100406w | *J. Phys. Chem. Lett.* **2010,** *1*, 1459–1462